J|A|C|S ARTICLES

Published on Web 11/19/2009

Nafion Structural Phenomena at Platinum and Carbon Interfaces

David L. Wood III,*,†,‡ Jerzy Chlistunoff,† Jaroslaw Majewski,§ and Rodney L. Borup†

Sensors and Electrochemical Devices Group, Materials Physics and Applications Division, MPA-11, MS D429, and Manuel Lujan, Jr. Neutron Scattering Center, LANSCE-LC, MS H805, Los Alamos National Laboratory, Los Alamos, New Mexico 87545

Received April 27, 2009; E-mail: wooddl@ornl.gov

Abstract: Neutron reflectometry was used to examine the interactions of polymer electrolyte fuel cell (PEFC) materials that comprise the triple-phase interface. Smooth, idealized layers of Nafion on glassy carbon (GC) and Pt surfaces were used to experimentally model the PEFC electrode interfaces. Different multilayer structures of Nafion were found in contact with the Pt or GC surfaces. These structures showed separate hydrophobic and hydrophilic domains formed within the Nafion layer when equilibrated with saturated D_2O vapor. A hydrophobic Nafion region was formed adjacent to a Pt film. However, when Nafion was in contact with a PtO surface, the Nafion at the Pt interface became hydrophilic. The adsorbed oxide layer caused a long-range restructuring of the perfluorosulfonic acid polymer chains that comprise Nafion. The thicknesses of the hydrophobic and hydrophilic domains changed to the same magnitude when the oxide layer was present compared to a thin hydrophobic domain in contact with Pt. A three-layer Nafion structure was formed when Nafion was in direct contact with GC. The findings in this research are direct experimental evidence that both the interfacial and long-range structural properties of Nafion are affected by the material with which it is in contact. Evidence of physical changes of aged Nafion films was obtained, and the results showed a permanent increase in the thickness of the Nafion film and a decrease in the scattering length density (SLD), which are attributed to irreversible swelling of the Nafion film. The aging also resulted in a decrease in the SLD of the GC substrate, which is likely due to either an increase in surface oxidation of the carbon or loss of carbon mass at the GC surface.

Introduction

Polymer electrolyte fuel cells (PEFCs) hold great promise for addressing the world's growing energy production problem due to their high efficiency, high energy density, high power density, and zero emissions. However, manufacturing of the individual components, in particular the porous composite electrodes, can be complex and expensive.[1−4] A membrane electrode assembly (MEA) is the active power-producing center of a PEFC and consists of anode and cathode catalyst layers coated onto either side of an ion-exchange polymer (or ionomer) membrane. The triple-phase interface of a PEFC electrode is comprised of three comingled interfaces—a Pt/C interface (for electron transport and catalyst particle dispersion), a Pt/ionomer interface (for proton transport to reaction sites), and an ionomer/C interface (for high dispersion of catalyst−support aggregates, electrode structural integrity, and high porosity for O_2/H_2 diffusion).[5−8] This work focuses on a commercially available ionomer, Nafion, which falls into the general class of perfluorosulfonic acid (PFSA) polymers. The molecular formula of the protonated form of Nafion is $C_{(2n+3m+4)}F_{(4n+6m+7)}O_{(m+4)}SH$, where n may vary between 6 and 13 depending on the equivalent weight (EW) of the ionomer, and $m \approx 1$.[9] Nafion contains a hydrophobic poly(tetrafluoroethylene) (PTFE) backbone with hydrophilic sulfonated, ether-containing side chains. Chemical structure representations have been summarized by Mauritz and Moore.[10]

Understanding the basic structure of PFSA ionomers is important for shedding light on water transport, proton transport, and the oxygen reduction reaction (ORR) mechanism occurring at the triple-phase interface. Phenomena such as proton transport through Nafion ion channels to the Pt surfaces and the related restructuring of Nafion to form the channels are of key interest. Water uptake is critical in forming these ion channels and plays

† Materials Physics and Applications Division.

‡ Current address: Materials Processing Group, Materials Science & Technology Division, Oak Ridge National Laboratory, P.O. Box 2008, MS 6083, Oak Ridge, TN 37831-6083.

§ Manuel Lujan, Jr. Neutron Scattering Center.

(1) Meyers, J. P. *Electrochem. Soc. Interface* **2008**, *17* (4), 36–39.
(2) Tsuchiya, H.; Kobayashi, O. *Int. J. Hydrogen Energy* **2004**, *29*, 985–990.
(3) Ralph, T. R.; Hards, G. A.; Keating, J. E.; Campbell, S. A.; Wilkinson, D. P.; Davis, M.; St.-Pierre, J.; Johnson, M. C. *J. Electrochem. Soc.* **1997**, *144*, 3845–3857.
(4) Barbir, F.; Gómez, T. *Int. J. Hydrogen Energy* **1997**, *22*, 1027–1037.
(5) Wilson, M. S.; Gottesfeld, S. *J. Appl. Electrochem.* **1992**, *22*, 1–7.
(6) Wilson, M. S.; Gottesfeld, S. *J. Electrochem. Soc.* **1992**, *139*, L28–L30.
(7) Wilson, M. S.; Valerio, J. A.; Gottesfeld, S. *Electrochim. Acta* **1995**, *40*, 355–363.
(8) O'Hayre, R.; Barnett, D. M.; Prinz, F. B. *J. Electrochem. Soc.* **2005**, *152*, A439–A444.
(9) Loppinet, B.; Gebel, G. *Langmuir* **1998**, *14*, 1977–1983.
(10) Mauritz, K. A.; Moore, R. B. *Chem. Rev.* **2004**, *104*, 4535–4585.

 10.1021/ja9033928

a key role in the ORR kinetics and mechanism. Furthermore, chemical decomposition is of great interest for the ionomer component of the electrode layers (to maintain high catalyst activity, electrochemical surface area, and reaction rates) and the ionomer membrane (to maintain sufficient open-circuit potential, to separate reactant gases, and to prevent cell failure). The interface between Pt nanoparticles and the catalyst support is critical from a Pt dispersion, electrocatalyst manufacturing, and electrode processing standpoint. From a durability perspective, understanding the processes involved with catalyst−support corrosion is important for preserving Pt−C contact and triple-phase integrity. Identifying these essential interfacial and structural phenomena and related degradation processes will help lead to improved electrode longevity and performance, as well as improved catalyst−support and membrane durability.

Neutron scattering has previously been used to examine the PEFC triple-phase interface by only one other research group[11] in addition to prior work reported by this group.[12] Neutron imaging has also been used to study the colloidal properties of dissolved PFSA membranes in dilute solutions,[9] to obtain liquid water distributions in operating PEFCs,[13−19] and to study the effects of subfreezing conditions on PEFC operation.[20] Neutrons provide several major advantages over X-ray and electron beams. Because they interact with the nuclei and not electron orbitals, neutrons provide excellent scattering contrast for light elements and sensitivity to isotopic substitution. Many low-Z elements have high neutron scattering cross sections, and isotopic substitution can be utilized to control contrast within a sample. For example, hydrogen has a slightly negative coherent scattering length, while the deuterium isotope has a large positive coherent scattering length. Exploitation of this particular isotopic dependence, through selective deuteration of hydrogenous materials to create contrast, has proven to be an invaluable tool for studying polymers and biological materials. Since the primary elemental constituents of our samples are hydrogen, carbon, oxygen, fluorine, sulfur, and platinum, high contrast is achieved by the neutron interactions and provides an excellent opportunity to study the electrode layers.

Neutrons can also penetrate bulky samples and experimental apparatuses. This is beneficial for experiments involving a controlled atmosphere, temperature exposure, and/or surface contact with a liquid. This is particularly useful in our experiments because structural and chemical changes of Nafion associated with in situ exposure to water molecules are of prime interest (requiring both a technique which can detect H or D atoms and a controlled environmental chamber). Finally, neutrons are capable of providing angstrom-level resolution as a function of sample depth, depending on the analytical method. Neutron reflectometry (NR) is a technique that was specifically developed to provide thickness resolution to several angstroms. The Pt and Nafion films used in this work were substantially thicker than several monolayers due to the film deposition techniques used. However, the difference in Nafion layer thickness between fuel cell electrodes (on the order of several monolayers) and the layers used in this work (on the order of tens of monolayers) is trivial because the interfacial regions are observable with angstrom-level resolution. In addition, it was desired to probe any effects of the substrate material on long-range morphological behavior of Nafion, which can only be done with thicker films.

Ultramicroelectrode studies were previously conducted with solution-cast thin-film Nafion/Pt interfaces. Results of these experiments showed that the Nafion morphology underwent restructuring in terms of the hydrophilic and hydrophobic components of the polymer. When Nafion was in contact with a bare Pt surface, the sulfonate-containing hydrophilic side chains were pushed away from the Pt surface. However, when a PtO monolayer was present, the hydrophobic backbone was pushed outward, and the hydrophilic side chains were in contact with the PtO surface. These restructuring processes were reversible and strongly influenced by the polymer hydration, as indicated by the effects of the relative humidity (RH), temperature, and equivalent weight of Nafion (i.e., inherent hydrophilicity of the polymer) on the electrochemical behavior of the Pt/Nafion interface.[21−23] These findings prompted the NR investigation discussed in this paper.

Experimental Methods

NR Measurement Technique. NR involves shining a “cold” (low-energy) neutron beam on a sample at a shallow angle and measuring the ratio of reflected to incident neutrons as a function of the momentum transfer vector. The surface profile analysis reflectometer (SPEAR) instrument used for the NR measurements has angstrom-level resolution to a depth of 3000−5000 Å with a preferred maximum depth range of 500−3000 Å (for details on the SPEAR instrument and neutron production method, see the Supporting Information). The raw data give the incident vector ($\vec{k}_{\mathrm{in}}$), reflectance vector ($\vec{k}_{\mathrm{out}}$), and scattering vector ($\mathbf{Q_z}$) according to

$$\vec{k}_{\mathrm{in}} - \vec{k}_{\mathrm{out}} = \mathbf{Q_z} = \frac{4\pi \sin\theta}{\lambda} \tag{1}$$

If a film is present, is uniformly applied, and has nonvanishing scattering contrast as compared with the substrate and the substrate is smooth, a plot of reflectivity (ratio of the scattered intensity to the intensity of the incident beam) vs scattering vector (Å^{-1}) yields defined Kissing fringes. These fringes originate from interference of the neutrons scattered from different interfaces. From a reflectivity plot of this type, the key properties of film thickness, substrate roughness, interfacial roughness, film scattering length density (SLD), and substrate SLD may be extracted. To obtain these parameters, a popular modeling program, Parratt32 (version 1.6, developed by C. Braun at the Hahn-Meitner-Institut Berlin), was used for this work. Parratt32 applies a best χ^2 fit to the experimental

(11) Murthi, V. S.; Dura, J. A.; Satija, S; Majkrzak, C. F. *ECS Trans.* **2008**, *16* (2), 1471–1485.
(12) Wood, D. L.; Chlistunoff, J.; Watkins, E. B.; Atanassov, P.; Borup, R. L. *ECS Trans.* **2006**, *3* (1), 1011–1021.
(13) Bellows, R. J.; Lin, M. Y.; Arif, M.; Thompson, A. K.; Jacobson, D. *J. Electrochem. Soc.* **1999**, *146*, 1099–1103.
(14) Satija, R.; Jacobson, D. L.; Arif, M.; Werner, S. A. *J. Power Sources* **2004**, *129*, 238–245.
(15) Trabold, T. A.; Owejan, J. P.; Jacobson, D. L.; Arif, M.; Huffman, P. R. *Int. J. Heat Mass Transfer* **2006**, *49*, 4712–4720.
(16) Owejan, J. P.; Trabold, T. A.; Jacobson, D. L.; Baker, D. R.; Hussey, D. S.; Arif, M. *Int. J. Heat Mass Transfer* **2006**, *49*, 4721–4731.
(17) Mukundan, R.; Davey, J. R.; Rockward, T.; Spendelow, J. S.; Pivovar, B. S.; Hussey, D. S.; Jacobson, D. L.; Arif, M.; Borup, R. L. *ECS Trans.* **2007**, *11* (1), 411–422.
(18) Spendelow, J. S.; Mukundan, R.; Davey, J. R.; Rockward, T.; Hussey, D. S.; Jacobson, D. L.; Arif, M.; Borup, R. L. *ECS Trans.* **2008**, *16* (2), 1345–1355.
(19) Hickner, M. A.; Siegel, N. P.; Chen, K. S.; Hussey, D. S.; Jacobson, D. L.; Arif, M. *J. Electrochem. Soc.* **2008**, *155*, B427–B434.
(20) Mukundan, R.; Davey, J. R.; Lujan, R. W.; Spendelow, J. S.; Kim, Y. S.; Hussey, D. S.; Jacobson, D. L.; Arif, M.; Borup, R. L. *ECS Trans.* **2008**, *16* (2), 1939–1950.
(21) Chlistunoff, J.; Uribe, F.; Pivovar, B. *ECS Trans.* **2006**, *1* (6), 137–146.
(22) Chlistunoff, J.; Uribe, F.; Pivovar, B. *ECS Trans.* **2007**, *2* (8)), 37–46.
(23) Chlistunoff, J.; Pivovar, B. *ECS Trans.* **2007**, *11* (1), 1115–1125.

data based on assumed values of thicknesses, roughnesses, and SLDs.

Sample Preparation. A fundamental requirement for any NR substrate is that it must be smooth—approaching atomically flat is ideal, as is nearly the case for a polished Si wafer. Regardless of the material type, the surface quality should be ≪100 Å root-mean-square (rms) roughness, or film fringes may not be visible in the raw data. Three different substrates for Nafion film deposition were used in this research: glassy carbon (GC), Pt-coated GC, and Si wafers. Details of the material selection and substrate preparation are given in the Supporting Information.

Nafion, 1100 EW, was used with the technique of spin coating to provide thin, smooth, and uniform films on the GC, Pt, or Si wafer surfaces (details of the coating process are provided in the Supporting Information). All films were either heat cured to 140 °C or annealed to 210 °C to simulate the decal electrode preparation method developed by Wilson and Gottesfeld.[5,6] Heat curing dries the Nafion of any residual water and alcohol from the simulated electrode layers. Only loosely aggregated Nafion particles are left behind after drying. The higher annealing temperature of 210 °C is above the glass-transition temperature range (160 °C for a dry Nafion 1100 EW membrane and 99 °C for a fully water-saturated one),[24] reorganizes the polymer chains, and causes a fusing effect of the Nafion aggregates within the film. Hensley et al. found that annealing thin, water-saturated Nafion membranes at 165 °C resulted in an increase in the crystallinity with an associated improvement in physical properties such as water and proton transport rates.[25] Morphological changes, i.e., an increase in crystallinity, were also confirmed by Moore and Martin only when annealing solution-cast Nafion films to high temperature (up to 185−190 °C).[26]

Pt films were prepared by radio frequency (RF) sputtering with exposure times to get thin films of ≤1200 Å. Details concerning the equipment and procedure used are given in the Supporting Information. The films produced were of high quality and had a smooth surface texture comparable to that of the GC substrates on which they were deposited.

Nafion Film Experimentation. To investigate effects of water content on in situ material phenomena of the Pt/Nafion interface, NR experiments were conducted with Nafion/Pt bilayer films deposited onto GC substrates. These samples were equilibrated with either ambient H_2O or high-purity D_2O vapors inside an airtight chamber (see the Supporting Information for details) and exposed to the neutron beam. The chambers were constructed of aluminum because of its low neutron SLD, which allows for the beam to pass through the chamber walls with little absorption.

Several of the Nafion/GC samples were aged after the initial NR measurements under accelerated conditions (80 °C DI water and air sparging gas) in special accelerated testing chambers, with experimental details given in the Supporting Information. These chambers were constructed with the express purpose of PEFC durability studies in a low-background-contamination environment where fuel cell operating conditions could be mimicked.

Results and Discussion

Reproducibility of the Nafion film preparation method was demonstrated with three different 1100 EW samples deposited onto a Si wafer (surface roughness ∼5 Å), which was used as the control substrate. These films were heat cured to ensure removal of excess volatiles. The Nafion SLDs and thicknesses were found to be $(4.03 \pm 0.06) \times 10^{-6}$ Å^{-2} and 607 ± 35 Å, respectively, with film−air roughnesses of 7−8 Å. Reflectivity

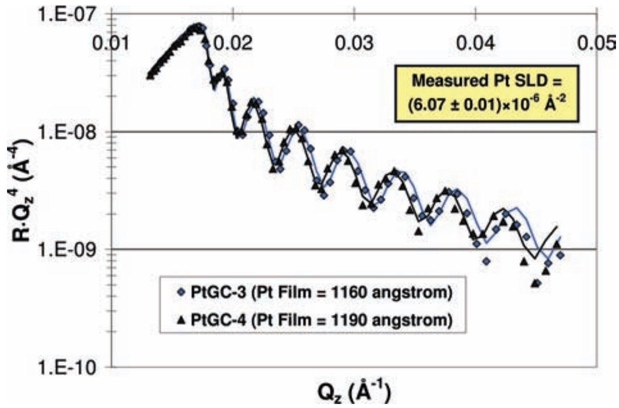

Figure 1. Modeled Pt film thicknesses and SLDs in terms of weighted NR profiles, i.e., $R\cdot\mathbf{Q_z}^4$ vs $\mathbf{Q_z}$ (lines are model fits). The reflectivity data are multiplied by $\mathbf{Q_z}^4$ and plotted versus $\mathbf{Q_z}$ to compensate for the sharp decrease in the reflectivity as described by Fresnel's law: $R \propto \mathbf{Q_z}^{-4}$.[27]

plots for the three Nafion 1100 EW films are given in the Supporting Information.

Reflectivity profiles weighted by $\mathbf{Q_z}^4$ (to compensate for the sharp decrease in reflectivity as described by Fresnel's law, $R \propto \mathbf{Q_z}^{-4}$)[27] together with their Parratt32 model fits are shown in Figure 1 for two different Pt/GC samples. Excellent agreement was found (1160 and 1190 Å—thicknesses within 2.5%) with SLDs of 6.08×10^{-6} and 6.06×10^{-6} Å^{-2}, respectively. The theoretical Pt metal SLD and bulk density are 6.35×10^{-6} Å^{-2} and 21.44 g/cm^3, so the sputtered Pt film SLD corresponds to 20.5 g/cm^3. The GC SLD was $(4.96 \pm 0.10) \times 10^{-6}$ Å^{-2}, which corresponds to a bulk density of 1.5 g/cm^3. The bulk density given by the manufacturer was 1.51 g/cm^3. A best-fit model to the data revealed that an intermediate Pt−C layer was present with an SLD between those of Pt and GC. This finding suggests that the Pt fully deposited into the ∼50 Å depth of surface roughness of the GC. (The surface roughness of the GC substrates was measured to be 50 ± 1 Å across six different samples.)

Material Characterization of Pt Films and GC Substrates. The outermost portions of the samples PtGC-3 and PtGC-4 (reflectivity data shown in Figure 1 for Pt on GC without a Nafion film) were characterized by XRD (the crystallograph for PtGC-3 is shown in the Supporting Information). The signal includes the entire Pt film thickness and the outer portion of the GC substrate. The XRD data were obtained for two main reasons: (1) identifying the predominant crystalline phases of the Pt and GC, which independently verified the material constituency of the film and substrate, and (2) determining the quality and reproducibility of the Pt deposition process and resultant film crystallography.

Both Pt and GC had preferred crystallographic orientations of Pt(111) and C(003), respectively. The Pt(111) and Pt(200) orientations comprised 83% and 9%, respectively, of the film structure (i.e., a 9.2:1 ratio). These results show that the sputtered Pt films are highly oriented in the Pt(111) orientation, as opposed to polycrystalline Pt, which has a 1.9:1 ratio of (111) to (200). The Pt(111) orientation is also the principal exposed phase in PEFC electrocatalysts,[28−31] which is based on the theoretical assumption of the cuboctahedral shape as the most surface energetically stable one.[32] As for the GC substrate, 59% of the

(24) Cho, K.-Y.; Jung, H.-Y.; Sung, K. A.; Kim, W.-K.; Sung, S.-J.; Park, J.-K.; Choi, J.-H.; Song, Y.-E. *J. Power Sources* **2006**, *159*, 524–528.
(25) Hensley, J. E.; Way, J. D.; Dec, S. F.; Abney, K. D. *J. Membr. Sci.* **2007**, *298*, 190–201.
(26) Moore, R. B.; Martin, C. R. *Macromolecules* **1988**, *21*, 1334–1339.
(27) Als-Nielsen, J. *Physica A* **1986**, *140*, 376–389.

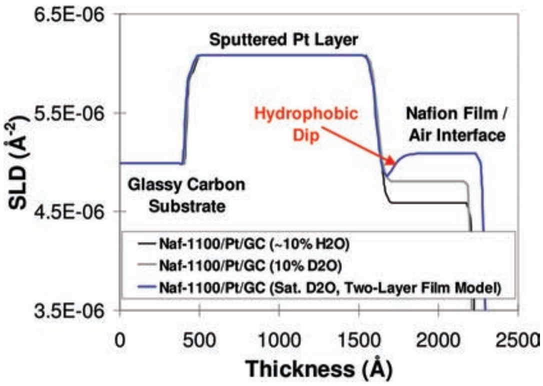

Figure 2. NR SLD profiles for the Nafion 1100/Pt bilayer system on the GC substrate in a saturated D_2O environment, a 10% D_2O environment, and ambient ~10% RH air. Note the film swelling of Nafion for the saturated D_2O case. The position of the GC/Pt interface was set at ~500 Å.

crystallinity was found to be of the (003) orientation. Only 21% and 7%, respectively, were identified as the (101) and (107) orientations, thus confirming that the GC also had preferred orientation. The C(003) *d* spacing was 3.47 Å, which is close to the acetylene black *d* spacing of 3.43 Å but greater than that of graphite (3.354 Å).[33] Carbon blacks with low graphitic content exhibit *d* spacings of 3.5−3.6 Å, which confirms that the GC material contained a significant degree of graphitic character since its *d* spacing was less than 3.5 Å.[33]

To investigate possible surface alteration effects from the O^- plasma etching process used to clean the GC substrates for the aging experiments, energy-dispersive spectroscopy (EDS) and water contact angle measurements (static sessile-drop method) were completed on control samples exposed to 0, 5, and 15 min of etching time (data provided in the Supporting Information). This etching environment is commonly used on Si wafers and is known to leave behind the same smooth ~3−5 Å SiO_2 layer initially present, as evidenced by before/after neutron and X-ray scattering. The O^- plasma increased the amount of adsorbed oxygen on the outermost layers of the GC. The EDS data showed no difference in adsorbed oxygen content between 0 and 5 min for the control samples, but it indicated about a ~20% increase with 15 min of exposure. A well-defined, decreasing trend of contact angle with increased plasma treatment time was obtained, though, and this finding confirms that the O^- environment increased the adsorbed oxygen content on GC even with only 5 min of exposure. The higher the oxygen content at the GC surface, the more hydrophilic character it exhibits; the water contact angle dropped from ~58° with 0 min of etching time to ~17° with 15 min of etching time. In the former case, there was only 3.8 atom % O at the surface, and in the latter case, there was 4.4 atom % O at the surface.

NR Data for Exposure of Nafion 1100/Pt Bilayer Films to D_2O. Figure 2 shows the SLD vs material thickness, known as an SLD profile, for a Nafion/Pt bilayer equilibrated with ~10% H_2O, 10% D_2O, and saturated D_2O (see sample PtGC-3 in Figure 1 for data corresponding to the sample without a Nafion film). When equilibrated with ambient ~10% RH air, the Nafion film thickness was 619 Å compared to 601 Å when equilibrated with 10% D_2O. The corresponding SLDs were 4.59×10^{-6} and 4.81×10^{-6} Å^{-2}, respectively, with the difference owed to the higher SLD of D_2O interpenetrating the polymer network. After equilibration with saturated D_2O (see Figure 2), the same parameters for a *homogeneous* Nafion layer were 693 Å and 4.93×10^{-6} Å^{-2}. However, for a good fit to the data the model required a two-layer *heterogeneous* Nafion film, suggesting a ~75 Å, relatively hydrophobic region (few or no D_2O molecules) with an SLD of 4.64×10^{-6} Å^{-2} adjacent to the Pt interface and a ~620 Å, relatively hydrophilic region (D_2O vapor equilibrated) with an SLD of 5.09×10^{-6} Å^{-2} adjacent to the vapor phase. The thin hydrophobic layer is evident in Figure 2 as a dip in the SLD (see the thick dark gray line).

In the work of Murthi et al.,[11] Pt and Au/Cr surfaces coated with Nafion were examined in vapor environments of different saturation levels, as well as in contact with liquid water. In contrast to the findings in this work, they did not find a heterogeneous Nafion film when equilibrating with 97% RH H_2O. Although a strong correlation among the Nafion film SLD, film thickness, and RH was found, it is thought that the difference in the Murthi et al. data and the data in this work is due to the difference in SLD between H_2O and D_2O. The decreasing trend in SLD with increasing RH found in their work may be due to Nafion film swelling, not scattering effects of

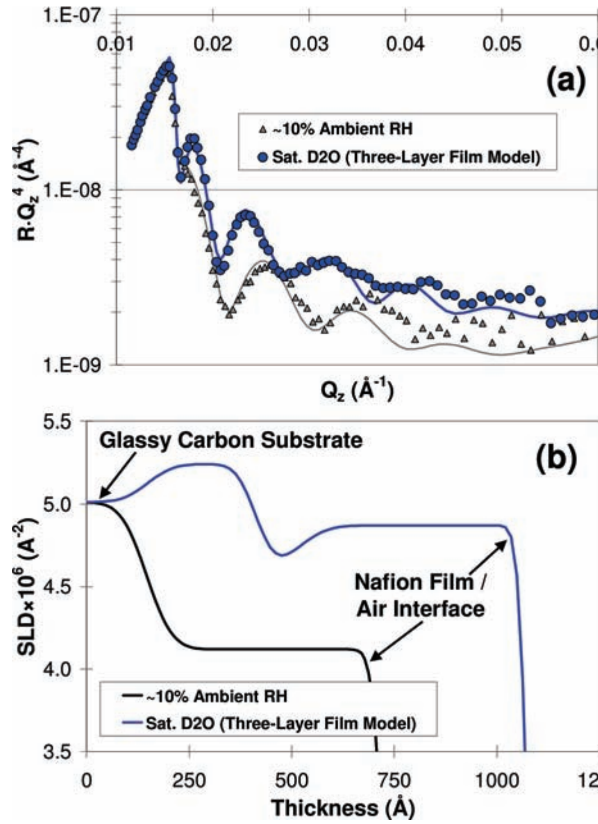

Figure 3. (a) Reflectivity profiles for Nafion 1100 EW films coated directly onto GC in saturated D_2O and ambient 10% RH H_2O environments. Lines are model fits. (b) SLD profiles show the film swelling in the saturated D_2O environment and corresponding three-layer NR model. The position of the GC/Nafion interface was set at ~0 Å.

(28) Markovic, N.; Gasteiger, H.; Ross, P. N. *J. Electrochem. Soc.* **1997**, *144*, 1591–1597.
(29) Joo, J. B.; Kim, P.; Kim, W.; Yi, J. *J. Electroceram.* **2006**, *17*, 713–718.
(30) Saha, M. S.; Gullá, A. F.; Allen, R. J.; Mukerjee, S. *Electrochim. Acta* **2006**, *51*, 4680–4692.
(31) Gancs, L.; Kobayashi, T.; Debe, M. K.; Atanasoski, R.; Wieckowski, A. *Chem. Mater.* **2008**, *20*, 2444–2454.
(32) Kinoshita, K. *J. Electrochem. Soc.* **1990**, *137*, 845–848.
(33) Kinoshita, K. *Carbon—Electrochemical and Physicochemical Properties*; John Wiley & Sons: New York, 1988; pp 31−33.

Table 1. Summary of Modeled Properties for Nafion 1100 EW Films Equilibrated with Saturated D_2O[a]

layer type	SLD (Å^{-2})	thickness (Å)	interfacial roughness (Å)
Nafion 1100/Pt/GC System (See Figure 2)			
outer more hydrophilic Nafion region	5.1×10^{-6}	619	20
inner less hydrophilic Nafion region	4.6×10^{-6}	74	63
Pt film	6.1×10^{-6}	1160	31
Nafion 1100/GC System (See Figure 3)			
outer less hydrophilic region	4.9×10^{-6}	577	21
middle "hydrophobic" region	4.6×10^{-6}	90	60
inner more hydrophilic region	5.2×10^{-6}	265	38
GC substrate	5.0×10^{-6}		49

[a] With and without an intermediate Pt film on a GC substrate.

increasing H_2O within the film (i.e., the SLD at room temperature of H_2O is only -5.58×10^{-7} Å^{-2}, and that of D_2O is 6.36×10^{-6} Å^{-2}). If this is the case, it would not be possible to accurately detect a heterogeneous Nafion film due to H_2O uptake with NR.

NR Data for Exposure of Nafion Films on Bare GC to D_2O. When the Nafion/GC samples (1100 EW without a Pt underlayer) were measured in a saturated D_2O environment, a different result and corresponding model were obtained. The weighted reflectivity profile is shown in Figure 3a for sample NGC-13, together with that of the 10% H_2O equilibrated profile for comparison. The data for the saturated D_2O case required a three-layer heterogeneous model to give reasonable agreement, consisting of a thin, rough intermediate "less hydrophilic" zone between two thicker, more hydrophilic layers (higher SLDs from higher D_2O contents). SLD profiles are shown in Figure 3b, and the three regions of the Nafion film are visible along with significant swelling (substantially larger thickness for the saturated D_2O case). The related difference in Kissing fringe spacing between the Nafion film equilibrated with 10% RH H_2O and saturated D_2O is evident in Figure 3a, with the saturated D_2O case exhibiting narrower fringe spacing and more marked fringe curvature. The hydrophilic layer adjacent to the vapor phase was about 2.2× thicker than that adjacent to the GC interface as seen in Figure 3b, and the total thickness of the three zones of the swollen Nafion film was ~930 Å—an increase of nearly 60%, agreeing well with the significant increases in SLD for all three zones. The film thickness for this sample when equilibrated with ambient air (~10% RH H_2O) was 587 Å, and the SLD was 4.12×10^{-6} Å^{-2}.

This substantial difference in SLD in the two different D_2O environments (see Figure 3b), as opposed to the smaller difference observed for a Nafion film coated onto Pt in the same two vapor environments (see Figure 2), is attributed to long-range bulk effects enacted by the differing contact materials. Note that the SLD of the Nafion 1100 EW film in the ~10% RH H_2O environment on GC was similar to that for the Si control substrate, 4.12×10^{-6} Å^{-2} vs $(4.03 \pm 0.06) \times 10^{-6}$ Å^{-2}, respectively, and considerably lower than that when in contact with the Pt film (i.e., 4.59×10^{-6} Å^{-2}). This difference is attributed to a densification of the Nafion film that occurred during the spin-coating or annealing processes when in the presence of Pt. Table 1 summarizes the individual layer thicknesses for both saturated D_2O cases shown in Figures 2 (Nafion in contact with Pt) and 3 (Nafion in contact with GC).

Repetition of Bilayer NR Measurements with a PtO Monolayer. The experiments conducted with varying RH environments discussed in the previous sections were repeated after conversion of the Pt surfaces (while still underneath the Nafion 1100 EW films) to a PtO monolayer. The methods used for electrochemical conversion were cyclic voltammetry and chronocoulometry. Details of the experimental procedure together with the cyclic voltammetry data are given in the Supporting Information. The same samples (PtGC-3 and PtGC-4 from Figure 1) were used to ensure that any changes in subsequent NR data were due to the addition of the PtO monolayer and not sample-to-sample variation.

In addition to giving quantitative information about the oxidized Pt surfaces, the cyclic voltammetry also provided information on the state of the reduced Pt surfaces in the preceding NR experiments. The initial potential cycle was rather featureless in both the anodic and cathodic directions. Subsequent potential cycles resulted in well-defined Pt oxidation and PtO reduction processes, involving ≥75% of the accessible Pt surface area in the second cycle (see the Supporting Information for experimental details). The low electrochemical activity of Pt in the first cycle likely had two sources: (i) blockage of the reduced Pt surface by the less hydrated (more hydrophobic) layer in Nafion (see above) and (ii) the low susceptibility of Pt(111), which was the predominant surface orientation for these samples, to oxidation at lower temperatures.[34,35] The significant increase in Pt activity in the subsequent cycles may be linked to the same phenomena. Liquid electrolyte (0.5 M H_2SO_4 used in this procedure) facilitates unblocking of the Pt surface,[21] thus rendering it more susceptible to oxidation.[36] This phenomenon makes it difficult to determine from the cyclic voltammetry data the fraction of surface that remained oxidized during the NR experiments with reduced Pt surfaces. However, the upper limit can easily be estimated. For the highest case scenario, if the cathodic current in the first cycle originated exclusively from PtO reduction, the respective electric charge would correspond to no more than 25% of the Pt surface having been in an oxidized state. The fraction of oxidized Pt surface would certainly have been less than this maximum value during the NR experiments prior to electrochemical surface conversion to PtO. Accordingly, it can be stated that the Pt surfaces of these samples were predominantly in the reduced state, and no significant effect of inherent PtO on the NR data could have been expected. As will be shown below, the NR results obtained for the oxidized Pt surfaces were different from those obtained for the reduced surfaces.

NR data are shown in Figure 4 comparing the SLD profiles of the PtGC-3 bilayer Nafion 1100/Pt film (without the oxide monolayer) and the trilayer Nafion 1100/PtO/Pt film in 100%

(34) Sashikata, K.; Furuya, N.; Itaya, K. *J. Vac. Sci. Technol., B* **1991**, *9*, 457–464.
(35) Markovic, N. M.; Ross, P. N., Jr. *Surf. Sci. Rep.* **2002**, *45*, 117–229.
(36) Motoo, S.; Furuya, N. *J. Electroanal. Chem.* **1984**, *172*, 339–358.

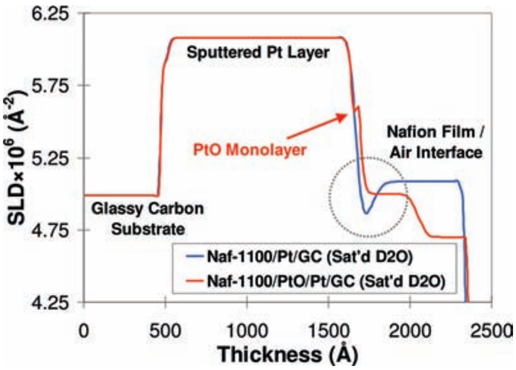

Figure 4. Comparison between SLD profiles of Nafion 1100 EW films coated onto sputtered Pt films with and without a PtO monolayer adjacent to the Nafion film, which was deposited via chronocoulometry (see the Supporting Information for procedural data and validation). All data above correspond to sample PtGC-3 (see Figure 1 for bare reflectivity data). The circle denotes different interfacial SLDs of Nafion adjacent to Pt. The position of the GC/Pt interface was set at ~500 Å.

RH D_2O. With the addition of the PtO monolayer, the domain of the Nafion film thickness adjacent to the Pt phase became hydrophilic (see the circled region in Figure 4), as evidenced by the absence of the hydrophobic dip in the SLD. The total thickness swelling of the Nafion film was about the same in each case—from 619 Å in 10% RH H_2O to 698 ± 4 Å in saturated D_2O. However, the thickness-weighted SLD of the Nafion film was significantly less with the presence of a PtO monolayer. This finding means that the total D_2O uptake in the Nafion film was proportionately less after the conversion of the Pt surface to oxide, which implies long-range restructuring of the Nafion and a lower capacity for water toward the film/air interface.

Changes in the thicknesses of the hydrophobic and hydrophilic domains of the heterogeneous Nafion model were also found, with near equality in the thicknesses of the two domains for the case with the PtO monolayer. Together these observations suggest that hydrophobic portions of the Nafion 1100 EW polymer chains are pushed away from the oxide interface. This means more $-SO_3^-$ end groups are present in the region of the Nafion film adjacent to PtO. This result is reasonable considering that PtO is more hydrophilic than Pt.[37] Furthermore, the data in Figure 4 indicate different long-range effects and polymer chain arrangement depending on whether a localized portion of Nafion within a PEFC electrode is in contact with Pt or PtO. These findings agree with historical data and hypotheses that have dealt with the subject of hydrophobic and hydrophilic PFSA domains.[38−42] Table 2 gives a summary of the SLDs, thicknesses, and interfacial roughnesses for the Nafion/Pt and Nafion/PtO/Pt profiles shown in Figure 4.

Murthi et al. observed a bilayer Nafion film when equilibrating the Pt and Au/Cr surfaces with liquid water.[11] X-ray reflectivity data showed the presence of a PtO film (determined to be <7 Å) on the Pt surface, and the NR data verified the presence of a thin hydrophilic Nafion region adjacent to the

(37) Li, Z.; Chang, S.-C.; Williams, R. S. *Langmuir* **2003**, *19*, 6744–6749.
(38) Tovbin, Y. K. *Zh. Fiz. Khim.* **1998**, *72*, 55–59.
(39) Yeager, H. L.; Steck, A. *J. Electrochem. Soc.* **1981**, *128*, 1880–1884.
(40) Hsu, W. Y.; Gierke, T. D. *J. Membr. Sci.* **1983**, *13*, 307–326.
(41) Tovbin, Y. K.; Vasyatkin, N. F. *Colloids Surf., A* **1999**, *158*, 385–397.
(42) Jang, S. S.; Molinero, V.; Çağin, T.; Goddard, W. A. *J. Phys. Chem. B* **2004**, *108*, 3149–3157.

Table 2. Summary of the SLD, Thickness, and Interfacial Roughness for a Nafion 1100/Pt Bilayer with and without a PtO Monolayer[a]

layer type	SLD (Å^{-2})	thickness (Å)	interfacial roughness (Å)
Nafion 1100/Pt/GC			
outer more hydrophilic region	5.1×10^{-6}	619	20
inner less hydrophilic region	4.6×10^{-6}	74	63
Pt film	6.1×10^{-6}	1160	31
Nafion 1100/PtO/Pt/GC			
outer less hydrophilic region	4.7×10^{-6}	333	12
inner more hydrophilic region	5.0×10^{-6}	372	43
PtO monolayer	4.4×10^{-6}	2	1

[a] The table values correspond to the SLD profiles in Figure 4.

PtO and a thick hydrophobic region in contact with air. This finding is in good agreement with the data presented in this work with the exception of the relative thicknesses of the hydrophilic and hydrophobic regions. This difference can be attributed to the use of H_2O in the Murthi et al. study and the use of D_2O in this study.

On the basis of the findings from this work, a concept of the polymeric structure near the Pt or PtO interface was envisioned. Any strong interactions between a smooth flat surface and either component of Nafion (hydrophilic side chains or hydrophobic backbone) are likely to lead to the polymer chains lying flat on that surface, which is completely different from Hsu and Gierke's model.[40] A sort of layering is likely for the studied interfaces due to a templating effect. The first layer of polymer chains interacts relatively strongly with the substrate. The second layer does not interact directly with the substrate, but the first layer acts like a template. As the hydrophobic and hydrophilic components in the second layer of polymer chains arrange themselves, they adhere to the corresponding hydrophobic and hydrophilic components in the first layer. The NR data suggest that a pseudoisotropic structure of Nafion (like that of Hsu and Gierke for a bulk membrane)[40] is modified and becomes anisotropic due to interactions with the substrate.

Correlation of NR and Cyclic Voltammetry Data. To confirm the NR layer modeling and conclusions, the results were compared with those of electrochemical studies employing Nafion-covered ultramicroelectrodes according to the method of Chlistunoff et al.[21] These studies indicate that partially hydrated, recast Nafion in contact with oxide-free Pt exhibits a tendency to push its hydrophobic component *toward* the Pt surface. The process of this ionomer restructuring was found to depend on the electrode potential and voltammetric scan rate and led to large hysteresis in the ORR voltammograms.[21] The long-range effects of the substrate type/state on Nafion interfacial structure, as indicated in Figures 2−4, are also evidenced by more recent electrochemical data. Figure 5 shows voltammograms recorded for Pt ultramicroelectrodes covered with Nafion films prepared in two different ways (slow and quick evaporation) and in the presence of 100% RH O_2 (Figure 5a) and 100% RH Ar (Figure 5b) at 20 °C. The significant difference between the ORR voltammograms in Figure 5a suggests different charge-transfer rates that could result from dissimilar arrangement of Nafion ionomer chains in direct contact with Pt. The nearly identical background currents (Figure 5b) taken in 100% RH Ar suggest long-range ionomer restructuring affecting oxygen transport to the Pt surface. The slight difference in background currents is limited to different magnitudes of oxidation/reduction currents of an Fe impurity (a reversible redox system at ~0.7

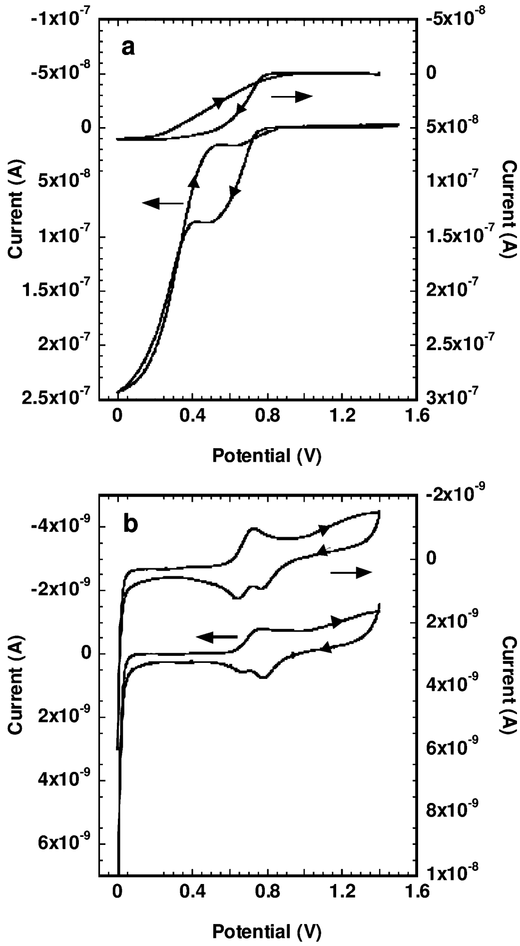

Figure 5. Effect of the film preparation method on the voltammetry of 100 μm Pt ultramicroelectrodes coated with Nafion in the presence of O_2 (a) and Ar (b) at 100% RH and 20 °C. The scan rate was 5 mV/s. The ionomer films were produced by a slow (top voltammograms) and quick (bottom voltammograms) evaporation of the Nafion solution (see ref 21 for the experimental procedure). Electrodes were equilibrated for 10 s at the anodic potential limit before the voltammograms were recorded.

V vs a hydrogen electrode utilizing 0.5 M H_2SO_4 and a forming gas, i.e., 6% H_2 in Ar), which is in qualitative agreement with the amount of Nafion solution used for film preparation. Fe impurities in Nafion are more pronounced in voltammograms at a slow scan rate of 5 mV/s (Figure 5),[23] but they are also known to have no effect on the ORR rate at a Pt/Nafion interface.[43,44] Results similar to those shown in Figure 5a for the quick evaporation were previously attributed to the enhanced water generation brought about by having thinner Nafion films (i.e., a reduced O_2 mass transport resistance resulting in higher ORR rates),[21] but that interpretation was not confirmed by the NR data discussed in the previous sections and the most recent electrochemical data.

Due to the complexity of the phenomena occurring at the Pt/Nafion interface during oxygen reduction,[21,22] it is difficult to unequivocally attribute the differences in oxygen voltammetry in Figure 5a to specific differences in the structure of the quickly and slowly evaporated films. The presence of oxygen during quick evaporation in air may cause partial oxidation of Pt, which can result in increased surface hydrophilicity and the formation of hydrophilic domains at the Pt/Nafion interface. A more random distribution of ionomer chains, which occurs during quick solvent evaporation, also increases the fraction of Pt surface area initially occupied by the hydrophilic component of Nafion. However, these phenomena do not significantly affect the response of the Nafion functional groups in the immediate vicinity of the Pt surface to the potential scan, as evidenced by the nearly identical voltammograms in Figure 5b. Consequently, the process of Nafion restructuring,[21,22] revealed by the hysteresis of the ORR voltammograms in Figure 5a, must affect the transport of oxygen to the reaction sites and involve deeper layers of Nafion. Oxygen transport and its changes during a potential scan are affected differently for the quickly and slowly evaporated Nafion films (Figure 5a) because the initial state of the Pt surface and the rate of film evaporation affect the film structure and its ability to reorganize at long distances from the Pt surface. From this perspective, the electrochemical results fully support the NR data, which demonstrate the long-range effects of the substrate on the Nafion structure. The presence of two relatively well-defined waves in both the forward and reverse scans of the oxygen voltammogram for the quickly evaporated film (Figure 5a) further suggests that the restructuring of quickly evaporated films is slower than that of slowly evaporated films. However, this effect is not expected to have had any influence on the NR data, which were obtained after at least 24 h of film equilibration time.

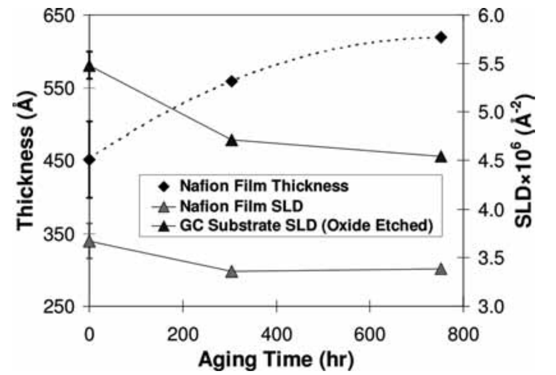

Figure 6. NR parameters of Nafion/GC samples (1100 EW films) as a function of the aging time in 80 °C DI water and air sparging gas.

Aging of Nafion Films on Bare GC. Nafion 1100 EW films were deposited onto bare GC substrates, which were then aged under simulated PEFC conditions (80 °C DI water and air sparging gas). The NR data after two different aging times are shown in Figure 6 compared to those for the samples prior to aging. A series of NR measurements made on nine different bare GC samples gave good reproducibility. An SLD and a roughness of $(4.96 \pm 0.10) \times 10^{-6}$ Å^{-2} and 53 ± 5 Å, respectively, were measured, which verified that the initial states of the GC substrate surfaces were similar.

A substantial increase in the Nafion film thickness of 38% was observed through ~750 h of aging, along with a simultaneous decrease in its SLD (see Figure 6). Under these accelerated testing conditions, the amount of free (or bulk) water appears to have increased during the aging process, which would have caused both film swelling and a reduction in bulk

(43) Okada, T.; Ayato, Y.; Dale, J.; Yuasa, M.; Sekine, I.; Asbjørnsen, O. A. *Phys. Chem. Chem. Phys.* **2000**, *2*, 3255–3261.
(44) Okada, T.; Ayato, Y.; Satou, H.; Yuasa, M.; Sekine, I. *J. Phys. Chem. B* **2001**, *105*, 6980–6986.

density.[45,46] The increased uptake of free water takes place in the hydrophilic domains of the Nafion structure, causing a morphological rearrangement between the hydrophobic backbone and hydrophilic side chains that ultimately leads to swelling. There is evidence that the thermal history affects the water uptake of Nafion, which is consistent with the conditions of the aging experiments performed in this work.[47] The Nafion SLD remained unchanged after about 300 h of aging, but the film surface roughness increased from 19 ± 3 Å (unaged samples) to 25 Å after ~300 h and up to 37 Å after ~750 h. The roughness increase is consistent with the morphological rearrangements Nafion undergoes after exposure to high-temperature liquid or vapor water. Both the decrease in SLD and the increase in film roughness with increased water uptake are in agreement with the findings of Murthi et al. for Nafion films on both Pt and Au/Cr surfaces (i.e., decreasing SLD was found with increasing RH).[11]

The Nafion 1100 EW SLDs for the fresh films in ambient 10% RH H_2O were lower than those deposited onto the control Si wafer and had a higher variability as well: $(3.67 \pm 0.18) \times 10^{-6}$ Å^{-2} for GC and $(4.03 \pm 0.06) \times 10^{-6}$ Å^{-2} for the Si wafers. They were also lower than that of the NGC-13 sample where the three-layer heterogeneous film modeling was done (i.e., 4.12×10^{-6} Å^{-2} in 10% RH H_2O). For the aging experiments, the GC substrates were treated with the O^- plasma for 15 min prior to spin coating of the films, whereas the GC substrate for the heterogeneous film modeling was not treated with O^- plasma. As discussed previously, the 15 min etching time made the GC surface substantially more hydrophilic (on the basis of the EDS and water contact angle data in the Supporting Information). This explains the difference in Nafion SLD for the same GC substrate, which is that there was a densification of the Nafion film for the case with lower surface O content.

The intent of this etching step was to clean the GC surface and decrease its surface roughness; however, the opposite happened concerning the roughness, which increased to an average value of 63 Å. The GC SLD also increased substantially to $(5.48 \pm 0.14) \times 10^{-6}$ Å^{-2}, a change indicative of a bulk density increase at the surface. The GC material used for this work had a nominal density of 1.51 g/cm^3 (corresponding to a measured average SLD value of $(4.9-5.0) \times 10^{-6}$ Å^{-2}), and the observed increase in SLD corresponds to a bulk density of 1.6−1.7 g/cm^3 (neglecting the effect of the increased surface concentration of oxygen). On the basis of the NR modeling and supplemental EDS and contact angle characterization, the plasma treatment cleaned the GC as desired at the expense of increasing the surface roughness, bulk density, and oxygen concentration.

Figure 6 also shows that a ~15% reduction in GC SLD occurred at the surface through ~750 h of aging, which corresponds to a reduction in bulk density to about 1.35 g/cm^3, a change in the carbon crystallographic structure to a less dense packing, an increase in oxygen content to about 25 atom %, or some combination of these effects. The GC SLD as a function of oxygen atomic concentration is given in the Supporting Information. It decreases with both decreasing bulk density and increasing oxygen content. Carbon corrosion at the surface layers of the GC would also lead to voids, which would correspond to a reduction in bulk density. This aging phenomenon is most likely a combination of effects and would be analogous to a loss of carbon mass from the electrocatalyst support within a PEFC electrode layer or an increase in hydrophilicity of the electrode carbon phase since it is well-known that surface-bound oxide reduces the hydrophobicity of carbon materials.

Conclusions

NR was used to examine the interactions of PEFC materials that exist at the triple-phase interface. Smooth, idealized layered models of Nafion on GC and Pt surfaces were used to experimentally model the PEFC electrode interfaces. Different multilayer structures of Nafion exist in contact with Pt or GC in a saturated D_2O environment. These structures show separate hydrophobic and hydrophilic domains formed within the Nafion layer. A hydrophobic Nafion region was formed adjacent to a Pt film, while a three-layer Nafion structure was formed with Nafion in direct contact with GC. When PtO was formed electrochemically on the same Nafion/Pt/GC samples, the Nafion at the Pt interface became hydrophilic. The oxide monolayer caused a long-range restructuring of the PFSA polymer chains. The thicknesses of the hydrophobic and hydrophilic domains changed to the same magnitude when the oxide layer was present, compared to a thin hydrophobic domain in contact with Pt. The findings in this research are direct experimental evidence that both the interfacial and long-range structural properties of Nafion are affected by the material with which it is in contact.

Nafion films deposited onto GC were examined before and after aging in accelerated testing chambers. The results showed a permanent increase in the thickness of the Nafion film and a decrease in the Nafion SLD, which were attributed to irreversible swelling of the Nafion film. The aging also resulted in a decrease in the SLD of the GC substrate, which was likely due to an increase in surface oxidation of the carbon, a loss of carbon mass at the GC interface, a rearrangement of the carbon crystalline surface structure, or a combination thereof.

Acknowledgment. The financial support of this work was provided in part by the U.S. Department of Energy (DOE) Fuel Cell Technologies Program (Program Manager Nancy Garland). This work was also supported by Los Alamos National Laboratory under DOE Contract W7405-ENG-36 and a grant from the DOE Office of Basic Energy Sciences under Award Number DE-FG02-04ER46173. We thank the Los Alamos Neutron Science Center (LANSCE) Nano-Engineering Program Advisory Committee for granting three consecutive beam-time awards on the SPEAR instrument. We thank Erik Watkins and Dhaval Doshi of the Manuel Lujan, Jr. Neutron Scattering Center for providing helpful suggestions, technical guidance, and raw-data analysis. We thank Roger Lujan for preparing the Pt-sputtered films.

Supporting Information Available: Figure S1, an exploded schematic of the SPEAR instrument, Appendix A, details of the neutron production method and flight path within SPEAR, Appendix B, substrate preparation for thin films, Appendix C, preparation of Nafion films by spin coating, Appendix D, Pt film deposition by the RF sputtering process, Appendix E, procedure for equilibrating the Nafion film with D_2O, Appendix F, aging procedure for Nafion/GC samples, Figure S2, reproducibility of the Nafion film spin-coating procedure via NR, Figure S3, XRD characterization of Pt and C phases for sample PtGC-

(45) Kim, Y. S.; Dong, L.; Hickner, M. A.; Glass, T. E.; Webb, V.; McGrath, J. E. *Macromolecules* **2003**, *36*, 6281–6285.
(46) Siu, A.; Schmeisser, J.; Holdcroft, S. *J. Phys. Chem. B* **2006**, *110*, 6072–6080.
(47) Onishi, L. M.; Prausnitz, J. M.; Newman, J. *J. Phys. Chem. B* **2007**, *111*, 10166–10173.

3, Figure S4, EDS and static sessile-drop contact angle characterization of the GC surface at different O^- plasma etching/cleaning times, Figure S5, cyclic voltammograms for determining the reduction charge of the PtO layer and associated monolayer coverage, Appendix G, experimental procedure for conversion of the Pt surface to a PtO monolayer, and Figure S6, GC SLD as a function of the bulk density at different atomic percentages of surface oxide. This material is available free of charge via the Internet at http://pubs.acs.org.

JA9033928